Development of a Miniature Air-bearing Stage with a Moving-magnet Linear Motor

Seung-Kook Ro[1,#] and Jong-Kweon Park[1]

1 Intelligent Machine Systems Research Center, Korea Institute of Machinery and Materials, Daejeon, South Korea, 305-343
Corresponding Author / E-mail: cniz@kimm.re.kr, TEL: +82-42-868-7115, FAX: +82-42-868-7180

KEYWORDS: Miniature air-bearing stage, Slotless linear motor, Magnetic preload, Micromachining tool

We propose a new miniature air-bearing stage with a moving-magnet slotless linear motor. This stage was developed to achieve the precise positioning required for submicron-level machining and miniaturization by introducing air bearings and a linear motor sufficient for mesoscale precision machine tools. The linear motor contained two permanent magnets and was designed to generate a preload force for the vertical air bearings and a thrust force for the stage movement. The characteristics of the air bearings, which used porous pads, were analyzed with numerical methods, and a magnetic circuit model was derived for the linear motor to calculate the required preload and thrust forces. A prototype of a single-axis miniature stage with dimensions of 120 (W) × 120 (L) × 50 (H) mm was designed and fabricated, and its performance was examined, including its vertical stiffness, load capacity, thrust force, and positioning resolution.

Manuscript received: December 4, 2007 / Accepted: December 10, 2007

1. Introduction

The miniaturization of machine tool systems provides many advantages by saving energy and space and by introducing flexibilities for manufacturing small parts. Machine tools that can be used in a micro-factory are being studied and developed worldwide, and some have been recently commercialized.[1,2] To build precise micro/mesoscale machine tools, the components, including the spindle, linear motion system, and tooling system, must be sufficiently small, precise, and stiff to satisfy the machine performance requirements.[3]

The choice of bearings and actuators are usually the main design considerations for the sliding system. A linear guide with a rolling element, such as a cross-roller guide or a ball screw drive, can be used for mesoscale machines. However, achieving the desired level of accuracy for positioning and motion at submicron levels is difficult, and such miniaturized devices are not affordable. A drive mechanism applying piezoelectric actuators has been used because of its compactness and fine stepping motions, but it suffers from low speeds and irregular motions.[2] Direct electromagnetic drives such as linear motors or voice coil motors have also been used for precision mesoscale machines.[7]

Linear motion stage systems with air bearings have been successfully applied to precision machining tools and measurement systems because air bearings have little friction.[4,5,6] These devices provide a high degree of positioning accuracy and low motion error through the use of area averaging on the guide error. Therefore, if they can be effectively miniaturized, air-bearing stages will provide good linear motion systems for precision micromachining tools.

A small air-bearing stage requires the following:

- small air bearings with sufficient load capacity and stiffness,
- a simple and light stage configuration, and
- a reasonably sized direct noncontact driving mechanism with an acceptable thrust force.

Air bearings with porous pads have larger load capacities than conventional orifice air bearings.[8] Moreover, porous material is easy to fabricate into aerostatic bearings, and the thickness of the porous pads can be reduced by applying an air-supply groove.[9]

Several configurations have been used for air-bearing stages. Rather than employing conventional wraparound or boxed preloading designs, we considered a magnetically preloaded design because it requires only one side of the guide surface in the preload direction. Examples in the literature include a case in which a magnetic preload with additional magnets was used for air bearings in precision linear stages and micromachining tools.[5,6] A magnetic preload can be generated from permanent magnets or by utilizing the attraction force of an iron-cored linear motor.[10]

Coreless linear motors with moving coils have been widely applied for air-bearing stages because they have no attraction forces and small cogging, but few models suitable for miniature stages are available. Iron-cored linear motors have larger thrust forces than coreless motors, but the variation in the attraction force caused by the magnet array and slots in the core can generate motion errors or cogging.[10] To overcome this, iron-cored motors without slots or slotless linear motors have also been used for drive mechanisms.[9-11] If the travel range is sufficiently small, a single-phase driving mechanism such as a voice coil motor can be used. Even though various linear motors and voice coil motors are available, few are small enough to be integrated in the middle of an air-bearing stage for a small machining tool, and thus an adequate driving mechanism must be developed.

In this study, a new air-bearing stage with a magnetic preload and

Copyright (c) 2008 by KSPE

a linear motor was developed for future use in micro-factory machining tools. The new air-bearing stage is unique in the sense that permanent magnets are used not only for the preload but also for the motion generation. The design and analysis method of the proposed air-bearing stage are described and experimental results from fabricated prototypes are presented.

2. Design and Analysis of the Miniature Air-Bearing Stage and Linear Motor

2.1 Overview of the proposed linear stage

A new air-bearing stage was devised in which a magnet array provides both the preload for the air bearing and the thrust force for the stage, as shown in Fig. 1. A single-pad air-bearing design with a magnetic preload was chosen, with no opposing air-bearing pads, so that only one side of the guide surface was required. This design provides a simple configuration and is advantageous for miniaturization. When a single-pad air bearing is used, an attraction force must be provided that acts as a preload against the repelling force of the airflow from the air bearing to obtain the desired clearance and stiffness. The attraction force between the permanent magnets and the stator back iron can be used for this purpose. In addition, if an electric current flow is supplied perpendicular to the direction of the attraction force (*i.e.* a magnetic field), Lorenz forces will occur. Since the back-iron core has no slot, the preload force should be constant.

The desired size of the single-axis stage was less than $120 \times 120 \times 50$ mm, with a maximum thrust force of 40 N and vertical stiffness of 18 N/μm.

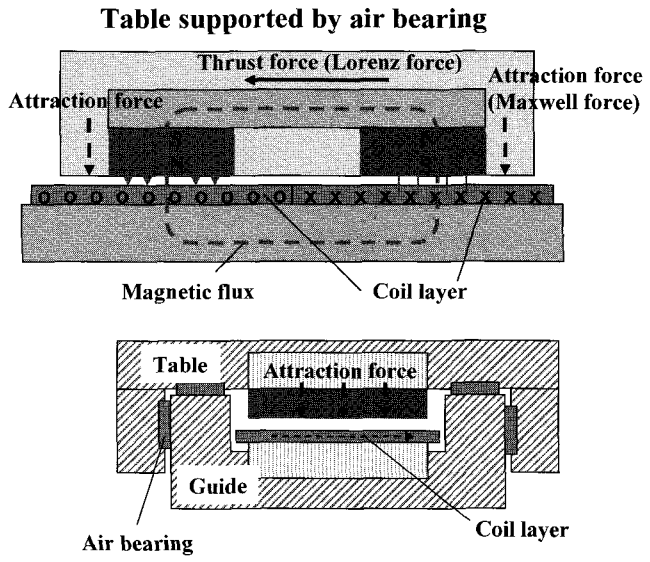

Fig. 1 Schematic diagram of an air-bearing stage with a slotless linear motor

2.2 Mathematic modeling of an air bearing with porous pads

The air bearings used in the proposed linear stage have rectangular porous pads with air-supply grooves (see Fig. 2). To calculate the load capacity, the pressure distribution at the porous pad face in the clearance must be determined by solving partial difference equations representing the three regions of the air bearing.[11] Inside the porous pad material, using Darcy's law and the state equation of gas and ignoring transient terms,

$$k_x \frac{\partial^2 p^2}{\partial x^2} + k_y \frac{\partial^2 p^2}{\partial y^2} + k_z \frac{\partial^2 p^2}{\partial z^2} = 0 , \tag{1}$$

where k_x, k_y, and k_z denote the permeability of the porous material in the x, y, and z directions, respectively. At the transition layer, using the mass flow rate equilibrium and considering the restriction constant E_z,

$$\begin{aligned} &-\frac{\rho k_x}{\mu}\frac{\partial p}{\partial x}\bigg|_{x-} dy\frac{dz}{2} - \frac{\rho k_y}{\mu}\frac{\partial p}{\partial y}\bigg|_{y-} dx\frac{dz}{2} \\ &-\frac{\rho k_z}{\mu}\frac{\partial p}{\partial z}\bigg|_{z-} dxdy \\ &= -\frac{\rho k_x}{\mu}\frac{\partial p}{\partial x}\bigg|_{x+} dy\frac{dz}{2} - \frac{\rho k_y}{\mu}\frac{\partial p}{\partial y}\bigg|_{y+} dx\frac{dz}{2} \\ &-\frac{\rho E_z k_z}{\mu}\frac{\partial p}{\partial z'}\bigg|_{z+} dxdy \end{aligned} , \tag{2}$$

where z' is the thickness of the restriction area. Finally, in the bearing clearance region, using the Navier–Stokes equations,

$$\frac{\partial}{\partial x}\left(h^3 \frac{\partial p^2}{\partial x}\right) + h^3 \frac{\partial^2 p^2}{\partial y^2} - 12 k_z E_z \frac{\partial p^2}{\partial z'} = 0 \cdot \tag{3}$$

These equations were evaluated with a numerical three-dimensional finite difference method.

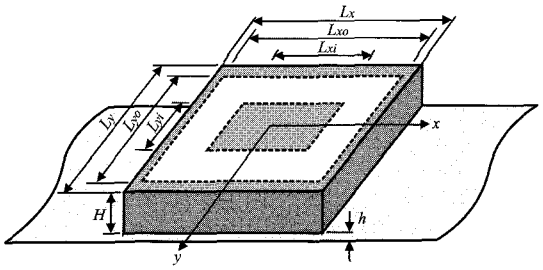

Fig. 2 Air-bearing pad made from a rectangular porous material

2.3 Modeling the magnetic forces acting on a linear motor

To obtain a simple configuration for the air-bearing stage, a motor with permanent magnets was introduced to provide both the thrust force and the preload force to the air bearings in the vertical direction. The forces acting on the proposed motor are described in Fig. 3. Two permanent magnets generated a constant magnetic flux at the air gap. The magnetic flux was concentrated to flow through the iron cores at the guide (base back iron) and the table (table back iron). Assuming that the flux density in the air gap is uniform in the vertical (Z) direction only, the magnetic force for the thrust and preload can be calculated using a magnetic circuit model.

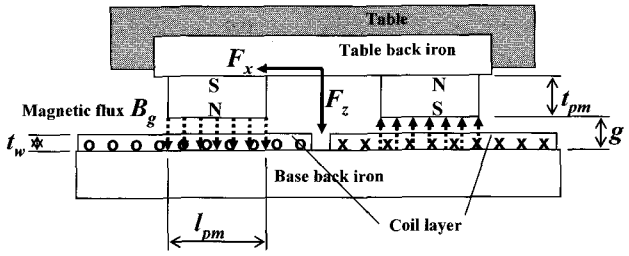

Fig. 3 Magnetic forces acting on the linear motor

The preload force F_z is generated by the Maxwell force, while the thrust force F_x is generated by the current in the coil layer due to the Lorenz force. Thus, the attraction force of an iron-cored linear motor

can be utilized for the air-bearing preload.

Since the magnetization of a permanent magnet made from a neodymium alloy (NdFeB) is almost linear, the B-H characteristics can be modeled as

$$B_{pm} = -\mu_{pm} H_{pm} + B_r, \tag{4}$$

where B_{pm} and H_{pm} are the flux density and magnetizing force in the permanent magnet, respectively, and B_r and μ_{pm} are the residual flux density and permeability, respectively, which are natural characteristics of the magnetic material that determine the strength of the magnet.

If the air-gap distance between the magnet face and stator back iron is g, the flux density in the air gap can be expressed based on magnetic circuit theory[15,16,17]

$$B_g = \frac{\mu_0 t_{pm} B_r}{(\mu_0 t_{pm} + \mu_{pm} g) K_l} \tag{5}$$

and the Maxwell force F_z can be calculated from

$$F_z = \frac{B_g{}^2 A_g}{\mu_0} = \frac{\mu_0 t_{pm}{}^2 B_r{}^2 A_g}{(\mu_0 t_{pm} + \mu_{pm} g)^2 K_l{}^2}. \tag{6}$$

The leakage factor K_l was applied to reduce the error caused by assuming a uniform flux. The leakage factor can be determined from the flux density distribution using a finite-element method or experiments; it is usually between 1.2 and 1.5. The dimensions of the magnets and air gap required to produce the preload force F_z can be determined from Equations (5) and (6).

For the thrust force, the Lorenz force can be expressed as

$$\vec{F} = \int \vec{B} \times \vec{J} dV \tag{7}$$

for an inductor carrying a current density J immersed in a magnetic field of density B within volume V. Using the same assumption of a constant uniform flux density, the thrust force acting on the magnets and table is

$$\begin{aligned} F_x &= 2B_g J A_g t_w \\ &= 2B_g J l_g w_g t_w \\ &= 2B_g w_g N I \end{aligned}, \tag{8}$$

where N is the number of turns immersed in the magnetic flux at area $t_w \times l_{pm}$, I is the current in the coil, and w_g and l_{pm} are the width and length of the magnets, respectively, so that the area of the air-gap face A_g is $l_{pm} \times w_g$. The thrust force of the motor is proportional to the flux density, current density, and volume of the coil immersed in the magnetic flux. From Equations (6) and (8), both the preload and thrust forces are primarily functions of the flux density B_g and gap area A_g. The current in the coil affects only the thrust force. By considering this relationship, the linear motor can be designed for the required preload and thrust force for a given current. For example, if the preload is fixed, or B_g and A_g are fixed, the thrust force can be increased by increasing the current density and coil volume. As the maximum current density is limited by the material characteristics of the coil and insulator, a larger coil volume or coil thickness of the coil layer t_w will give a larger thrust force, but the coil thickness cannot be larger than the air gap g.

2.4 Results of the air-bearing analysis

The size of the porous air-bearing pad was determined to be 25 × 16 × 4 mm. The air-supply groove dimensions were L_{xo} = 19 mm, L_{xi} = 9 mm, L_{yo} = 10 mm, and L_{yi} = 4 mm. The pads for the vertical bearings were placed in a 2-row by 3-column arrangement considering the size of the table and guide rail. Figure 4 shows the calculated load capacity and stiffness of the porous pad for supply pressures of 0.4 and 0.5 MPa. The permeability of the porous material was $k_x = k_y = 1 \times 10^{-15}$ m^2 and $k_z = 3 \times 10^{-15}$ m^2. The air-supply area correction was applied by changing the width of the air-supply groove by 2 mm. The required vertical preload was determined from the load capacity at a given clearance with a desirable stiffness value. For example, with six pads, a preload of 120 N was required to obtain a clearance of 13 μm when the stiffness was 21.4 N/μm.

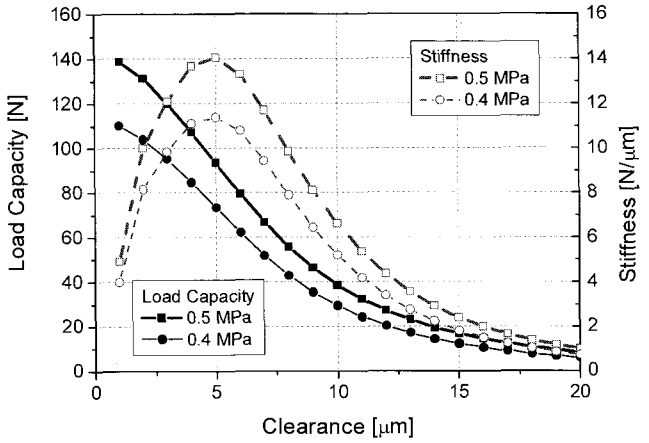

Fig. 4 Calculated load capacity and stiffness of a porous air-bearing pad

2.5 Preload and thrust of the linear motor

Two brick-shaped NdFeB 33 MOe-grade permanent magnets (B_r = 1.17 T, $H_c = 8.597 \times 10^6$ A/m), $w_{pm} \times l_{pm} \times t_{pm} = 40 \times 20 \times 10$ mm, were placed in the motor as shown in Fig. 3. When the dimensions of a magnet are fixed, the preload and thrust forces are affected by the air gap g and the coil size and density. Figure 5 shows the flux density of the air gap B_g and preload force F_z calculated using the magnetic circuit model. A leakage factor of K_l = 1.3 was obtained from a two-dimensional finite element analysis using ANSYS 9.0. The flux density of the air gap was 0.4 to 0.55 T for air gaps of 6 to 14 mm, which is acceptable for iron cores.

Figure 6 shows the continuous and peak thrust force when the current density was 10 A/mm^2 for the continuous force and 20 A/mm^2 for the peak force. These current density values are equivalent to 1.96 A and 3.92 A, respectively, for a 0.5-mm-diameter wire. The thickness of the coil layer, t_w, was 4 mm. For g = 10 mm, the resultant continuous and peak forces were 19 N and 38 N, respectively.

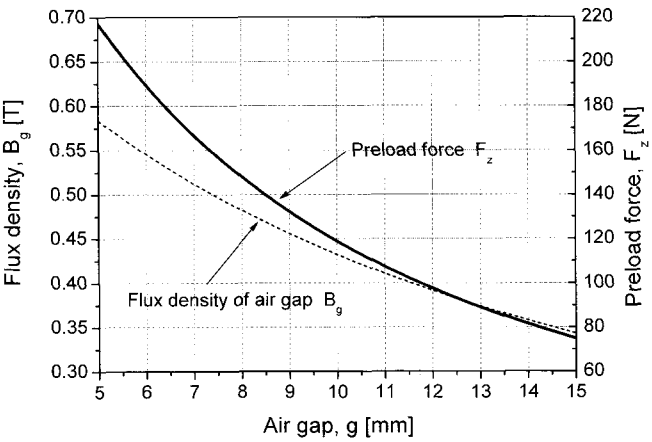

Fig. 5 Magnetic flux density and preload force of the linear motor calculated from the magnetic circuit model (K_l = 1.3)

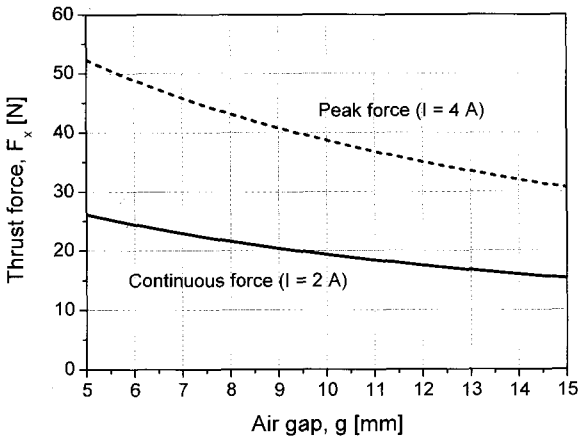

Fig. 6 Peak and continuous thrust force (t_w = 4 mm)

From the analysis, a single-axis prototype was designed, as shown in Fig. 7. The specifications are listed in Table 1. The air gap g was determined to be 10 mm. A single-phase control was used for the motor coil over the 20-mm travel range.

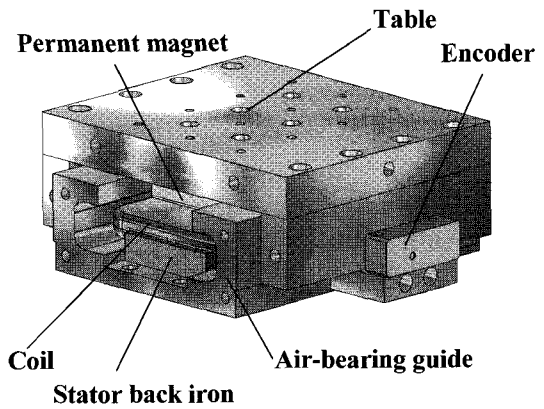

Fig. 7 Single-axis miniature air-bearing stage with a linear motor

Table 1 Design parameters for the miniature air-bearing stage

Size (W × L × H)	120 × 120 × 50 mm
Stroke	20 mm
Permanent magnet	2 EA (40 × 20 × 10 mm)
Air-bearing clearance (vertical)	13 μm
Vertical air-bearing stiffness	21.4 N/μm
Magnetic preload (vertical)	120 N
Table weight	0.98 kg
Encoder resolution	50 nm
Thrust force (Continuous/Peak)	20 N/40 N

3. Experimental Results for the Air-Bearing Stage

3.1 Fabrication of the single-axis prototype

A prototype stage was fabricated as shown in Fig. 8. The base rail and table were made of aluminum alloy with a hard coating, and carbon porous pads were used for the air bearings. The coil for the slotless linear motor was wound on a bobbin and attached to the stator iron core. The total number of turns of the 0.5-mm-diameter copper wire used for the coil was 460, and the measured resistance of the coil was 8.9 Ω. An optical encoder with a 50-nm resolution (Renishaw RGH25) was introduced for the positioning control. The coil was driven by a PWM amplifier with an internal current feedback loop, and its position was controlled by a digital controller.

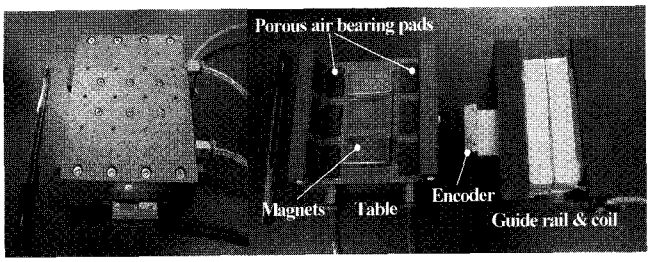

Fig. 8 Fabricated miniature air-bearing stage with a slotless linear motor

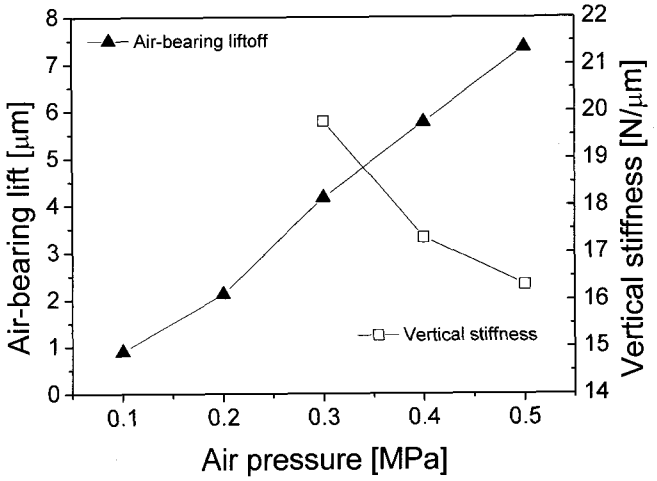

Fig. 9 Air-bearing clearance and stiffness of the table

3.2 Clearance and stiffness of the air bearings

The clearance of the air bearings was determined by measuring the liftoff distance from the table with capacitive sensors (ADE-3401). Figure 9 shows the liftoff at the center of the table for 0.1 to 0.5 MPa of supplied air pressure and the vertical stiffness measured by deflection when small known weights were applied. At 0.5 MPa, the clearance was 7.5 μm and the corresponding vertical stiffness was 16.5 N/μm. Since differences existed in the load capacity and stiffness values between the analysis and experiment, some parameters used in the air-bearing calculations, such as the permeability of the porous material, were in error, or local deformations occurred in the guide or table. At a smaller air pressure, 0.3 MPa, the vertical stiffness almost reached the desired value of 20 N/μm with a smaller clearance.

Some large differences were observed between the simulated and experimental air-bearing clearances. These may have been due to the reduction in air-supplying area of the air-bearing pads as a result of the adhesive spreading while bonding the pad to the pocket. If the spreading depth of the adhesive is assumed to be 2 mm, the air-supplying area will be reduced by 50%; this will decrease the load capacity and stiffness of the air bearings. Hence, future designs should have wider air-supplying areas to provide more load capacity.

3.3 Thrust force of the linear motor

The thrust force was measured with a load cell by applying currents of up to 3 A to the coil with a regulated DC power supply. The stage was positioned at three locations: the center, and at 5 and 10 mm (end position). The results are shown in Fig. 10. The force rate with respect to the input current was 10.15 N/A at the center with good linearity. This force rate was reduced to 8.15 N/A when the stage was at the end position (10 mm) because the flux at the air gap was not straight due to a fringing flux at the corner of the magnets. Thus, the actual area passing through the magnetic flux was reduced by the end of the stator iron core. The maximum peak flux density, 0.56 T, was measured with a gauss meter. The average flux density

was 0.43 T, which coincides with the two-dimensional finite element results. This demonstrates the validity of the magnetic circuit model for calculating the preload and thrust forces of the proposed linear motor.

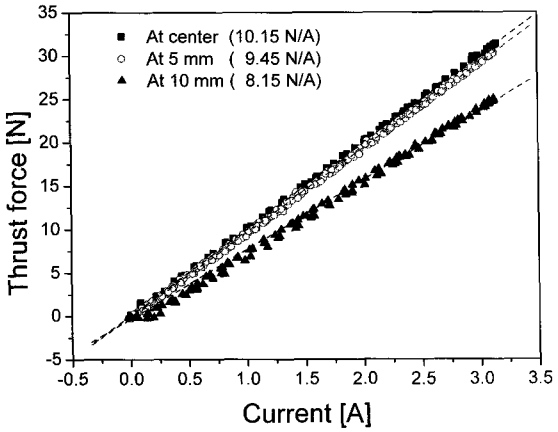

Fig. 10 Measured thrust force due to the current

The temperatures of the coil, table, and rail were measured during the experiment and are shown in Fig. 11. The temperature of the coil increased to 60°C. Since the temperature limit of a commercial linear motor coil subjected to a continuous force is 100°C, a continuous force of 20 N is acceptable for the proposed linear motor.

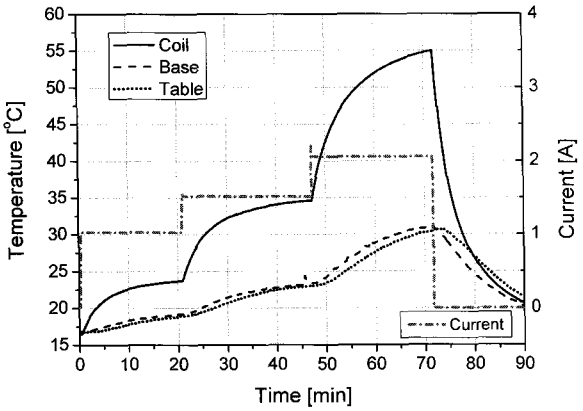

Fig. 11 Temperature rise of the stage due to the motor coil current

3.4 Positioning control test

A PWM power amplifier (Copley Controls, 4122Z) integrated with a current feedback circuit and a compact digital controller (Delta-Tau PC104, PMAC2-based system) were used for the positioning control system. The bandwidth of the current control with the PWM amplifier was set to 1.5 kHz. Figure 12 shows the results of a rapid movement test after manually tuning the PID gains. A rapid velocity of 50 mm/s and an acceleration of 5 m/s^2 were possible, which were sufficient for this application considering the total stroke length of 20 mm.

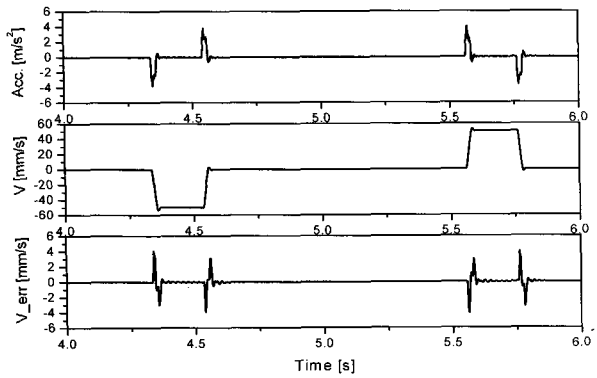

Fig. 12 Rapid positioning results (10 mm movement with 50 mm/s velocity)

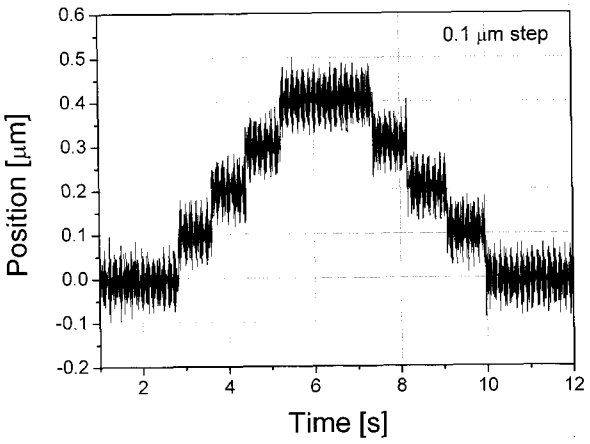

Fig. 13 Fine positioning with 0.1-μm step commands (0.05 μm of encoder resolution)

Figure 13 shows the fine step response of 0.1-μm commands measured with a capacitive gap sensor (ADE 3401). The stage oscillated for only one pulse of the encoder resolution, yielding a resolution of 0.1 μm. We believe that the positioning accuracy could be improved by using a linear encoder with a finer resolution, e.g., 10 nm.

4. Conclusions

We proposed a miniature air-bearing stage that was integrated with porous air-bearing pads. A cored moving-magnet linear motor provided the thrust and preload forces for the air bearings in the vertical direction. Mathematic models for the linear motor and porous air bearings were derived and used to design a single-axis prototype that was 120 × 120 × 50 mm in size with a travel range of 20 mm. The prototype was fabricated and tested. The air-bearing clearance was 7.5 μm, the vertical stiffness was 17.5 N/μm at 0.5 MPa, and the continuous thrust force was estimated at 20 N for 2 A, as desired. Since the air bearings produced almost no friction, the positioning resolution was 0.1 μm with a linear encoder resolution of 0.05 μm. This resolution could be improved by using an encoder with a finer resolution. This stage system is suitable for building miniature machining tools for future use in micro-factory systems, which will require miniaturized air-bearing stages and actuators.

ACKNOWLEDGMENT

The research presented in this paper was performed as part the "Development of Microfactory System Technology for the Next Generation" project sponsored by MOCIE, South Korea.

REFERENCES

1. Okazaki, Y., Mishima, N. and Ashida, K., "Microfactory-Concept, History, and Developments," Journal of Manufacturing Science and Engineering, Vol. 126, Issue 4, pp. 837–844, 2004.

2. Vogler, M. P., Liu, X., Kapoor, S. G., DeVor, R. E. and Ehmann, K. F., "Development of Meso Scale Machine Tool (mMT) Systems," Transactions of NAMRI/SME, Vol. 30, pp. 653–661, 2002.

3. Smith, S. T. and Seugling, R. M., "Sensor and Actuator Considerations for Precision, Small Machines," Precision Engineering, Vol. 30, Issue 3, pp. 245–264, 2006.

4. Hwang, J. H., Park, C. H. and Kim, S. W., "Estimation of 2D Position and Flatness Errors for a Planar XY Stage Based on

Measured Guideway Profiles," International Journal of Precision Engineering and Manufacturing, Vol. 8, No. 2, pp. 64-69, 2007.

5. Ro, S. K., Kim, S. H., Kwak, Y. G. and Park, C. H., "Linear Air Bearing Stage with Actively Controllable Magnetic Preload," Conference Proceedings of EUSPEN, pp. 297–300, 2006.
6. Ro, S. K., Park, J. K., Yoon, H. S. and Ehmann, K. F., "Static and Dynamic Characteristics of Magnetically Preloaded Stages for a 3-Axis Micro-Machine Tool," Proceedings of the KSMTE Spring Conference, pp. 468–472, 2005.
7. Fukada, S. and Nishimura, K., "Nanometric Positioning Over a One-Millimeter Stroke Using a Flexure Guide and Electromagnetic Linear Motor," International Journal of Precision Engineering and Manufacturing, Vol. 8, No. 2, pp. 49-53, 2007.
8. Fourka, M. and Bonis, M., "Comparison between Externally Pressurized Gas Thrust Bearings with Different Orifice and Porous Feeding System," Wear, Vol. 210, Issue 2, pp. 311–317, 1997.
9. Yoshimoto, S. and Kohno, K., "Static and Dynamic Characteristics of Aerostatic Circular Porous Thrust Bearings (Effect of the Shape of the Air Supply Area)," ASME Journal of Tribology, Vol. 123, Issue 3, pp. 501–508, 2001.
10. Slocum, A., Basaran, M., Cortesi, R. and Hart, A. J., "Linear Motion Carriage with Aerostatic Bearings Preloaded Inclined Iron Core Linear Electric Motor," Precision Engineering, Vol. 27, Issue 4, pp. 382–394, 2003.
11. Park, C. H. and Lee, H., "Motion Error Analysis of the Porous Air Bearing Stage Using the Transfer Function," Journal of Korean Society for Precision Engineering, Vol. 21, No. 7, pp. 185–194, 2004.
12. Filho, A. F. F., Susin, A. A. and da Silveria, M. A., "An Analytical Method of Predicting the Static Performance of a Planar Actuator," IEEE Transactions on Magnetics, Vol. 39, No. 5, pp. 3364–3366, 2003.
13. Basak, A. and Anayi, F. J., "A DC Linear Motor with a Square Amarture," IEEE Transactions on Energy Conversion, Vol. 10, No. 3, pp. 462–469, 1995.
14. Basak, A., Filho, A. F. F., Nakata, T. and Takahasi, N., "Three-dimensional Computation of Force in a Novel Brushless DC Linear Motor," IEEE Transactions on Magnetics, Vol. 33, No. 2, pp. 2030–2032, 1997.
15. Furlani, E. P., "Permanent Magnet and Electro-mechanical Devices: Materials, Analysis and Applications," Academic Press, 2001.
16. Lee, S. H., Baek, Y. S. and Jung, K. S., "Modeling and Analyzing Electromagnets for Magnetic Suspension Systems, "International Journal of Precision Engineering and Manufacturing, Vol. 7, No. 4, pp. 28-33, 2006.
17. Fitzgerald, A. E., Kingsly, C., Jr. and Umans, S. D., Electric Machinery, McGraw–Hill, 1992.